

Parallelization of the FFT on $SO(3)$ ¹

DENIS-MICHAEL LUX, Lübeck University

CHRISTIAN WÜLKER², Department of Mechanical Engineering, Johns Hopkins University

GREGORY S. CHIRIKJIAN, Department of Mechanical Engineering, Johns Hopkins University

In this paper, a work-optimal parallelization of Kostelec and Rockmore’s well-known fast Fourier transform and its inverse on the three-dimensional rotation group $SO(3)$ is designed, implemented, and tested. To this end, the sequential algorithms are reviewed briefly first. In the subsequent design and implementation of the parallel algorithms, we use the well-known Forster (PCAM) method and the OpenMP standard. The parallelization itself is based on symmetries of the underlying basis functions and a geometric approach in which the resulting index range is transformed in such a way that distinct work packages can be distributed efficiently to the computation nodes. The benefit of the parallel algorithms in practice is demonstrated in a speedup- and efficiency-assessing benchmark test on a system with 64 cores. Here, for the first time, we present positive results for the full transforms for the both accuracy- and memory-critical bandwidth 512. Using all 64 available cores, the speedup for the largest considered bandwidths 128, 256, and 512 amounted to 29.57, 36.86, and 34.36 in the forward, and 24.57, 26.69, and 24.25 in the inverse transform, respectively.

ASM CCS concepts: • **Mathematics of computing** → Computation of transforms;

Additional key words and phrases: fast Fourier transform, rotation group, parallel computing, fast rotational matching, OpenMP

1. INTRODUCTION

Computational harmonic analysis on the three-dimensional rotation group $SO(3)$ has many applications in industry and the natural science disciplines. In the technique of *fast rotational matching*, for example, one tries to find the rotation under which a given object resembles another object as closely as possible [Kovacs and Wriggers 2002]. The meaning of ‘resemblance’ between two objects is here determined by the specific context. In electron microscopy (EM), for instance, it can be the aim to fit an available high-resolution structure from X-ray crystallography or nuclear magnetic resonance (NMR) spectroscopy into the reconstructed three-dimensional EM image [Bhamre et al. 2015; Fabiola and Chapman 2005; Kam 1980]. On the other hand, computational harmonic analysis on $SO(3)$ can be used in *molecular replacement* to solve the phase problem in X-ray crystallography [Storoni et al. 2004; Navaza 1993; Crowther 1972]. Another application of fast rotational matching in the field of molecular biology is *virtual drug screening* [Mavridis et al. 2007]. Here, the goal is to maximize the overlap of the electron density functions of two given biomolecules, *e.g.*, by a mass-center-aligned purely rotational search. The concomitant determination of the maximal overlap is used to evaluate the structural resemblance of both molecules. In this way, it is possible to draw conclusions about similarities in the features of the molecules. Rotating a biomolecule against another also forms an essential part in the related field of *protein-protein docking* (see, *e.g.*, [Bajaj et al. 2013, 2011; Garzon et al. 2009; Ritchie et al. 2008]). The problem of optimal three-dimensional rotation alignment has been addressed in the field of computer graphics [Kazhdan 2007], too, where also rotation-invariant shape descriptors are of interest [Kazhdan et al. 2003]. Reversely, the problem can be to estimate a rotation, say, from spherical images [Makadia and Daniilidis 2006; Makadia et al. 2004]. Last but not least, computational spectral analysis on $SO(3)$ plays an important role in computational harmonic analysis on the three-dimensional Euclidean motion group $SE(3)$ [Kyatkin and Chirikjian 2000].

¹ Our C++ implementation is available from the corresponding author.

² Corresponding author (christian.wuelker@jhu.edu)

The fast Fourier transform on $SO(3)$ (hereinafter abbreviated as FSOFT) and its inverse (iFSOFT) introduced by Kostelec and Rockmore [2008] nowadays constitute an integral part of many techniques based on, including, or related to fast rotational matching (see [Bülow and Birk 2011a,b] for examples in robotics and automation, [Slabaugh et al. 2008] for an example in industrial design, and [Baboud et al. 2011; Makadia and Daniilidis 2010; Makadia et al. 2007] for examples in computer vision/-graphics). However, a parallelization of these computationally demanding algorithms has not yet been undertaken and presented (though it is noteworthy that protein-protein docking has been accelerated using graphic processors [Macindoe et al. 2010; Ritchie and Venkatraman 2010]). In this sense, the aim of this work is to design and implement such parallelization of the FSOFT and iFSOFT, and to demonstrate the practical applicability of the resulting parallel algorithms.

The remainder of this paper is organized as follows: Firstly, in Section 2, we briefly review the mathematical theory of the three-dimensional rotation group $SO(3)$ and corresponding discrete Fourier transform. The FSOFT and iFSOFT are then revisited. Subsequently, in Section 3, the parallelization of the sequential algorithms is carried out. Here, we use the Forster (a.k.a. PCAM) method [1995], as well as the OpenMP standard (www.openmp.org). Our parallelization is based on symmetries of the underlying basis functions and a geometric approach in which the resulting index range is transformed so as to allow for an efficient distribution of distinct work packages to the available computation nodes. Section 4 contains the benchmark test by means of which we demonstrate the practical benefits of our parallelization using our freely available implementation. In Section 5, we discuss the results and give an outlook on future developments.

2. PRELIMINARIES

The aim of this section is to familiarize the reader with the sequential fast $SO(3)$ Fourier transform and its inverse of Kostelec and Rockmore [2008], in order to prepare for the parallelization in Section 3. By those already familiar with the FSOFT and iFSOFT, this section can be skipped. In Subsection 2.1, the three-dimensional rotation group $SO(3)$ is defined. We then introduce the corresponding basis functions, called Wigner- D functions, in Subsection 2.2. In Subsection 2.3, the discrete $SO(3)$ Fourier transform and its inverse are described. The fast $SO(3)$ Fourier transform and its inverse are revisited in Subsection 2.4.

2.1. $SO(3)$

The algebraic group $SO(3)$ of rotations in three-dimensional real space consists of all orthogonal real-valued 3×3 matrices with determinant one, *i.e.*,

$$SO(3) := \{R \in \mathbb{R}^{3 \times 3} \mid R^T R = E_3, \det R = 1\},$$

where E_3 denotes the 3×3 identity matrix. Each such matrix R is called a *rotation*, because multiplication of a three-dimensional vector (in Cartesian coordinates) by R results in a rotation of this vector around a certain rotation axis. In this context, the group operation (composition) of two rotations is simply matrix multiplication. There are three elementary rotation matrices, R_x , R_y , and R_z , describing rotations about the x , y , and z axis, respectively. For a given rotation angle $\alpha \in [0, 2\pi)$, they are given by

$$R_x(\alpha) := \begin{bmatrix} 1 & 0 & 0 \\ 0 & \cos \alpha & -\sin \alpha \\ 0 & \sin \alpha & \cos \alpha \end{bmatrix}, \quad R_y(\alpha) := \begin{bmatrix} \cos \alpha & 0 & \sin \alpha \\ 0 & 1 & 0 \\ -\sin \alpha & 0 & \cos \alpha \end{bmatrix}, \quad R_z(\alpha) := \begin{bmatrix} \cos \alpha & -\sin \alpha & 0 \\ \sin \alpha & \cos \alpha & 0 \\ 0 & 0 & 1 \end{bmatrix}.$$

In the following, we use the so-called z - y - z *Euler-angle decomposition*, which is a particular way of parameterizing $SO(3)$. In this decomposition, only two of the above ele-

mentary rotation matrices are required, namely R_y and R_z : *To each rotation* $R \in \text{SO}(3)$ *we can assign Euler angles* $\alpha \in [0, 2\pi)$, $\beta \in [0, \pi]$, *and* $\gamma \in [0, 2\pi)$, *such that*

$$R = R(\alpha, \beta, \gamma) = R_z(\gamma)R_y(\beta)R_z(\alpha).$$

2.2. Wigner-D functions

In this section, we introduce the so-called *Wigner-D functions*, which are special functions mapping from SO(3) to the set of complex numbers. These functions can be defined using the Euler angles introduced above as

$$(1) \quad D(l, m, m'; \alpha, \beta, \gamma) := \exp(-im\alpha) d(l, m, m'; \beta) \exp(-im'\gamma),$$

where $l \geq 0$ and $m, m' = -l, \dots, l$, while $d(l, m, m')$ denotes the respective real-valued *Wigner-d function*

$$\begin{aligned} d(l, m, m'; \beta) &:= (-1)^{m+m'} \sqrt{\frac{(l+m')!(l-m)!}{(l+m)!(l-m)!}} \\ &\times \left(\sin \frac{\beta}{2}\right)^{m'-m} \left(\cos \frac{\beta}{2}\right)^{m+m'} P(l-m'; m'-m, m+m'; \cos \beta), \end{aligned}$$

where $P(l-m'; m'-m, m+m')$ denotes the standard Jacobi polynomial of degree $l-m'$ and with exponents $m'-m$ and $m+m'$ (cf. [Abramowitz and Stegun 1972, Eq. 22.2.1]). The Wigner-D functions serve as the basis functions for the discrete and fast SO(3) Fourier transform, playing essentially the same role as the monomials $\exp(ikx)$ in the classical discrete Fourier transform (DFT).

In the following, we consider the linear spaces spanned by the Wigner-D functions with l less than a fixed $B \geq 1$,

$$H_B := \text{span}\{D(l, m, m') : l < B; m, m' = -l, \dots, l\}.$$

These linear combinations of Wigner-D functions are called *bandlimited functions* with *bandwidth* B . Each space H_B is a finite-dimensional subspace of the space $L^2(\text{SO}(3))$ of functions square-integrable over SO(3), inheriting the inner product

$$\langle f, g \rangle := \int_0^{2\pi} \int_0^\pi \int_0^{2\pi} f(\alpha, \beta, \gamma) \overline{g(\alpha, \beta, \gamma)} d\alpha \sin \beta d\beta d\gamma,$$

where \bar{g} denotes the complex conjugate of g . It can be shown that the Wigner-D functions satisfy the orthogonality relation [Kostelec and Rockmore 2008, Eq. 2.7]

$$\langle D(j, k, k'), D(l, m, m') \rangle = \frac{8\pi^2}{2l+1} \delta(j, l) \delta(k, m) \delta(k', m').$$

Here, δ denotes the standard Kronecker-delta symbol. The Wigner-D functions with $l < B$ thus form an *orthogonal basis* of H_B . This property is crucial, because the orthogonality of the Wigner-D functions allows to determine the unique Fourier representation of functions $f \in H_B$ by computing the inner products of f with the basis elements $D(l, m, m')$ for $l < B$ (as explained in the upcoming Section 2.3). The most important property of the Wigner-D functions in the context of harmonic analysis on SO(3) is the fact that *the Wigner-D functions constitute an orthogonal basis of* $L^2(\text{SO}(3))$.

To close this section, we collect some useful properties of the Wigner-d functions, which will later be used to evaluate these functions numerically in an efficient manner. The Jacobi polynomials are orthogonal polynomials. As such, they satisfy a *three-term recurrence relation*. Since the particular Jacobi polynomial $P(l-m'; m'-m, m+m')$ is

included in the Wigner- d function $d(l, m, m')$ as a factor, we find that when $l \geq 1$,

$$(2) \quad d(l+1, m, m'; \beta) = \frac{(l+1)(2l+1)}{\sqrt{((l+1)^2 - m^2)((l+1)^2 - (m')^2)}} \left(\cos \beta - \frac{mm'}{l(l+1)} \right) d(l, m, m'; \beta) \\ - \frac{(l+1)\sqrt{(l^2 - m^2)(l^2 - (m')^2)}}{l\sqrt{((l+1)^2 - m^2)((l+1)^2 - (m')^2)}} d(l-1, m, m'; \beta).$$

The following initial cases seed this recursion:

$$d(m, \pm m, m'; \beta) = \sqrt{\frac{(2m)!}{(m+m')!(m-m')!}} \left(\cos \frac{\beta}{2} \right)^{m \pm m'} \left(\pm \sin \frac{\beta}{2} \right)^{m \mp m'}, \\ d(m', m, \pm m'; \beta) = \sqrt{\frac{(2m')!}{(m'+m)!(m'-m)!}} \left(\cos \frac{\beta}{2} \right)^{m' \pm m} \left(\mp \sin \frac{\beta}{2} \right)^{m' \mp m}.$$

The Wigner- d functions also present some useful symmetries [Edmonds 1996, P. 59 f.]:

$$(3) \quad d(l, m, m'; \beta) = (-1)^{m-m'} d(l, -m, -m'; \beta) \\ = (-1)^{m-m'} d(l, m', m; \beta) \\ = (-1)^{l-m'} d(l, -m, m'; \pi - \beta) \\ = (-1)^{l+m} d(l, m, -m'; \pi - \beta) \\ = (-1)^{l-m'} d(l, -m', m; \pi - \beta) \\ = (-1)^{l+m} d(l, m', -m; \pi - \beta) \\ = d(l, -m', -m; \beta).$$

2.3. Discrete SO(3) Fourier transform

Let a bandwidth $B \geq 1$ be fixed. Functions f on SO(3) with bandwidth B , i.e., functions $f \in H_B$, possess a unique *Fourier representation*

$$(4) \quad f = \sum_{l=0}^{B-1} \sum_{m, m'=-l}^l f^\circ(l, m, m') D(l, m, m'),$$

where the (generalized) *Fourier coefficients* $f^\circ(l, m, m')$ are given by

$$f^\circ(l, m, m') := \frac{2l+1}{8\pi^2} \langle f, D(l, m, m') \rangle.$$

The discrete SO(3) Fourier transform and its inverse, and hence also the FSOFT and iFSOFT, are based on the following SO(3) *sampling theorem* [Kostelec and Rockmore 2008, Thm. 1]:

Let $f \in H_B$. The Fourier coefficients $f^\circ(l, m, m')$ of f obey the quadrature formula

$$(5) \quad f^\circ(l, m, m') = \frac{2l+1}{8\pi B} \sum_{i, j, k=0}^{2B-1} w_B(j) f(\alpha_i, \beta_j, \gamma_k) \overline{D(l, m, m'; \alpha_i, \beta_j, \gamma_k)}, \quad |m|, |m'| \leq l,$$

with the sampling angles $\alpha_i := i\pi/B$, $\beta_j := (2j+1)\pi/4B$, $\gamma_k := \alpha_k = k\pi/B$, and the quadrature weights

$$(6) \quad w_B(j) := \frac{2\pi \sin \beta_j}{B^2} \sum_{i=0}^{B-1} \frac{\sin((2i+1)\beta_j)}{2i+1}.$$

In the algorithmical context, any algorithm for computation of the Fourier coefficients $f^\circ(l, m, m')$ of functions $f \in H_B$ based on (5) is referred to as a *discrete SO(3) Fourier transform*. Correspondingly, reconstruction of the function values $f(\alpha_i, \beta_j, \gamma_k)$ from the Fourier coefficients $f^\circ(l, m, m')$ via (4) is called an *inverse discrete SO(3) Fourier transform*.

2.4. Fast SO(3) Fourier transform

As can be seen with Gauss' well-known formula for the sum of the first n positive integers, a function f on SO(3) with bandwidth B possesses $B(4B^2 - 1)/3$ potentially non-zero Fourier coefficients. One-by-one computation of these Fourier coefficients by evaluating the triple sum in (5) requires a total of $\mathcal{O}(B^6)$ computation steps. This is unacceptable for most practical purposes.

By a *separation of variables*, Kostelec and Rockmore [2008] reduced this complexity: Inserting the expression (1) into (5) and rearranging the summands yields

$$f^\circ(l, m, m') = \frac{2l+1}{8\pi B} \sum_{j=0}^{2B-1} w_B(j) d(l, m, m'; \beta_j) \underbrace{\sum_{i,k=0}^{2B-1} f(\alpha_i, \beta_j, \gamma_k) \exp(i(m\alpha_i + m'\gamma_k))}_{=: S(m, m'; j)}.$$

The following procedure lends itself well to this particular structure: In a first step, for all fixed $j = 0, \dots, 2B - 1$, the inner sum $S(m, m'; j)$ is computed for all $m, m' = 1 - B, \dots, B - 1$ with a standard two-dimensional iFFT. This requires a total of $\mathcal{O}(B^3 \log B)$ steps. Then, for all fixed $m, m' = 1 - B, \dots, B - 1$, the Fourier coefficients $f^\circ(l, m, m')$, $l = \max\{|m|, |m'|\}, \dots, B - 1$, are computed. Due to the three-term recurrence relation (2) of the Wigner- d functions, this can be done in $\mathcal{O}(B^4)$ operations using, for example, the well-known Clenshaw algorithm [Clenshaw 1955], or in even only $\mathcal{O}(B^3 \log^2 B)$ steps by using a fast discrete polynomial transform (FDPT, see [Potts et al. 1998; Driscoll et al. 1997]). The symmetries (3) can be used to speed up this second step. This, however, will not have an impact on the complexity. The complexity of the above-described sequential FSOFIT thus amounts to $\mathcal{O}(B^4)$ or even only $\mathcal{O}(B^3 \log^2 B)$.

In order to describe the corresponding fast inverse transform, we bring the second step above into matrix-vector notation. For this, let

$$V_B(m, m') := \text{diag}[(2l+1)/8\pi B]_{l=\max\{|m|, |m'|\}, \dots, B-1},$$

$$T_B(m, m') := [d(l, m, m'; \beta_j)]_{\substack{l=\max\{|m|, |m'|\}, \dots, B-1 \\ j=0, \dots, 2B-1}},$$

$$W_B := \text{diag}[w_B(j)]_{j=0, \dots, 2B-1}.$$

Then, for all fixed $m, m' = 1 - B, \dots, B - 1$, it is

$$\begin{aligned} [f^\circ(l, m, m')]_{l=\max\{|m|, |m'|\}, \dots, B-1} &= V_B(m, m') T_B(m, m') W_B [S(j; m, m')]_{j=0, \dots, 2B-1}, \\ [S(j; m, m')]_{j=0, \dots, 2B-1} &= T_B(m, m')^T [f^\circ(l, m, m')]_{l=\max\{|m|, |m'|\}, \dots, B-1}. \end{aligned}$$

Multiplication by the matrix $V_B(m, m') T_B(m, m') W_B$ is called the *discrete Wigner transform* (DWT) of orders m and m' for the bandwidth B . Multiplication with the transposed matrix $T_B(m, m')^T$ is thus referred to as the *inverse discrete Wigner transform* (iDWT). It is easy to see how the iDWT and a two-dimensional FFT constitute the sequential iFSOFIT, which has the same complexity as the FSOFIT, when the iDWT is realized correspondingly with an adjoint Clenshaw algorithm or an adjoint FDPT.

3. PARALLELIZATION

We use the well-known Forster method [1995] to design our parallel FSOF. The Forster method is also known as the PCAM method, which is an abbreviation for the four successive phases of *partitioning*, *communication*, *agglomeration*, and *mapping*, of which Forster's method is comprised. For more information on this method, we refer the reader to [Quinn 2003; Roosta 2000; J 1992]. Once the parallel FSOF is designed, the corresponding parallel iFSOF can be deduced from it directly. We shall not discuss parallelization of the two-dimensional FFT/iFFT, for this is not our concern (see Sects. 4 & 5).

Partitioning. As explained above, in the second step of the FSOF, the DWT has to be performed for all different orders $m, m' = 1 - B, \dots, B - 1$. This m - m' partitioning is reasonably fine.

Communication. As regards the underlying mathematics, a single DWT does not require any information of or from another DWT, and there is thus no such communication necessary between the threads. However, it clearly makes sense to exploit the seven Wigner- d symmetries (3) in order to speed up the computations. This results in communication between eight DWTs each, except for when $m = 0, m' = 0$, or $m = m'$. In these cases, the DWT groups are smaller, because not all seven Wigner- d symmetries (3) are meaningful here.

Agglomeration. Drawing the required DWTs for a bandwidth B into a two-dimensional m - m' integer coordinate system reveals a quadratic area with side length $2B - 1$. A direct approach for agglomeration would be to cluster the DWTs with respect to m or m' to groups of $2B - 1$ each. However, as indicated above, pursuing such straightforward strategy would effectively prevent us from making use of the Wigner- d symmetries (3). We thus agglomerate the DWTs based on these symmetries to groups of eight or less instead. No communication is required between these groups.

Mapping. Since the distinct work packages of eight DWTs or less are relatively small, we assign them one-by-one to the available computation nodes, as explained in the following.

Drawing all the DWT clusters into the same coordinate system as above results in a triangular area to be worked through; on the code level, this is represented by two nested 'for' loops: $m = 0, \dots, B - 1$ and $m' = 0, \dots, m$. Using Gauss' formula for the sum of the first n positive integers, the two indices m and m' can be mapped bijectively onto a single linear index

$$(7) \quad \sigma := \frac{m(m+1)}{2} + m'.$$

This has the apparent advantage that the arising 'for' loop over $\sigma = 0, \dots, B(B+1)/2$ can easily be worked through by the nodes. However, when reconstructing

$$(8) \quad \begin{aligned} m = m(\sigma) &= \left\lfloor \sqrt{2\sigma + \frac{1}{4} - \frac{1}{2}} \right\rfloor, \\ m' = m'(\sigma) &= \sigma - \frac{m(\sigma)(m(\sigma) + 1)}{2}, \end{aligned}$$

floating-point arithmetic is required and square roots are to be taken.

By a purely geometric approach, we can transform the above-described triangular index range bijectively into a rectangular area in such a way that reconstruction of the indices m and m' is less complicated. Our idea is illustrated in Fig. 1. Here, we assume that the bandwidth B is odd; however, the following formulae are also valid for an even bandwidth. The indices $m = 1, \dots, B - 1$ and $m' = 1, \dots, m - 1$ can be reconstructed

from the indices $i = 1, \dots, \lfloor (B-1)/2 \rfloor$ and $j = 1, \dots, B-1$ introduced in Fig. 1 via

$$m = m(i, j) = \begin{cases} B-i & \text{if } j > i, \\ i+1 & \text{otherwise,} \end{cases}$$

$$m' = m'(i, j) = \begin{cases} B-j & \text{if } j > i, \\ j & \text{otherwise} \end{cases}$$

(for B odd and $i = (B-1)/2$ only the values $j = 1, \dots, (B-1)/2$ are actually needed). Note that only a conditional ‘if’ statement and integer arithmetics are required here, as opposed to in (8). The indices i and j can now be mapped bijectively onto a single linear index (cf. (7))

$$\kappa := (i-1)(B-1) + (j-1),$$

so that they can be reconstructed via

$$i = i(\kappa) = \left\lfloor \frac{\kappa}{B-1} \right\rfloor + 1,$$

$$j = j(\kappa) = \text{mod}(\kappa, B-1) + 1.$$

Here, only integer division as well as modulus and increment operations are required. The resulting ‘for’ loop over $\kappa = 0, \dots, (B-1)(B-2)/2$ can now be parallelized, so that the DWT clusters are distributed efficiently to the available computation nodes.

The thus finished parallel FSOFIT scales well with the problem size and the number of available computation nodes. The reason for this lies within the small size of the working packages and the fact that there is no communication required between the working threads. This in turn yields a high locality of the data. Memory access of the different nodes can be made exclusive, in the sense that each node works in its own memory range. Furthermore, the fine granularity of the working packages makes it easy for the compiler to find a good scheduling. As indicated above, it is now clear how to derive the corresponding parallel iFSOFIT. With some additional effort, it can be shown that the above-described parallel FSOFIT and its inverse are *work-optimal* (cf. [JáJá 1992, P. 32]) – see [Lux 2015, Sec. 2.5] for proof.

4. BENCHMARK TEST

In the following, we describe the benchmark test by means of which we demonstrate the practical benefits of our parallel FSOFIT and iFSOFIT. This test assesses the speedup and the efficiency of the parallel algorithms. The *speedup* is approximated by the comparison ratio of the runtime of the parallel FSOFIT/iFSOFIT and the corresponding fast sequential algorithm (cf. [Quinn 2003; JáJá 1992]). The *efficiency* can then be determined as the ratio of the speedup and the number of computation nodes employed (ebd.). All measurements were performed with our C++ implementation. The test system was an x86 64-Bit Linux cluster (OpenSuse 13.1) with an AMD Opteron 6272 CPU ($4 \times 16 = 64$ cores) and 128 GB of RAM. We used OpenMp to realize our parallel design. The DWT and iDWT were realized as direct matrix-vector multiplication, were all the Wigner- d symmetries (3) were exploited in the pre-computation of the matrices using the three-term recurrence relation (2) (see also Sec. 5). Extended double precision (80-Bit x86 extended precision format) was used instead of double precision for the DWT/iDWT. Dynamic scheduling was enabled using the OpenMP directive `schedule(dynamic)`. We constructed a simple parallel two-dimensional FFT/iFFT from the one-dimensional sequential FFT/iFFT of the well-known Fastest Fourier Transform in the West (FFTW) using OpenMP as suggested by the developers (<http://www.fftw.org/parallel/parallel-fftw.html>; see also Sec. 5).

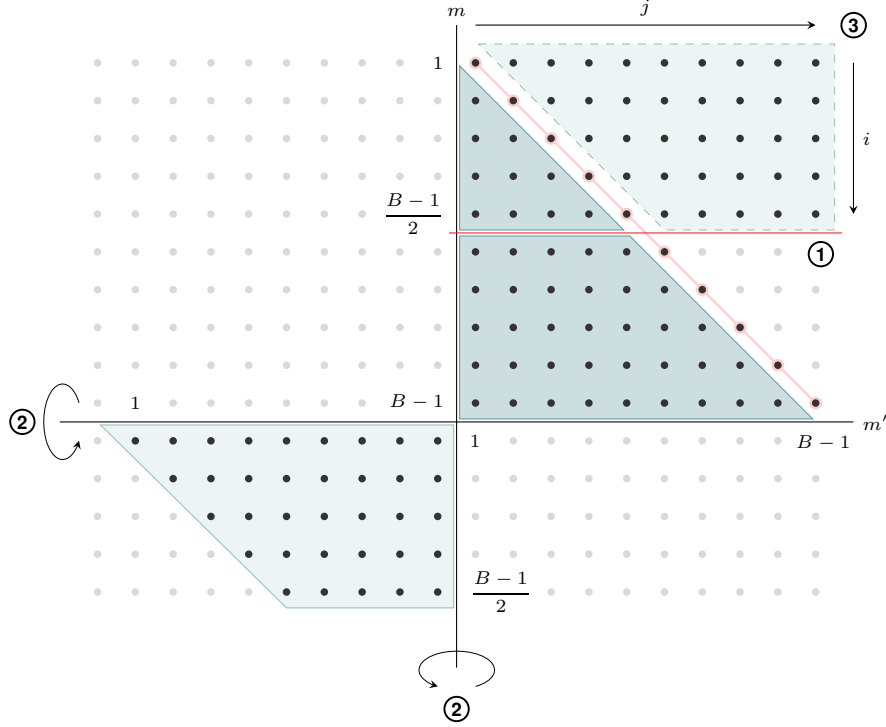


Fig. 1. Geometric approach for optimization of the nested ‘for’ loops over $m = 0, \dots, B - 1$ and $m' = 0, \dots, m$. The triangular area shaded in darker green contains the groups of DWTs for all combinations of m and m' for a given odd bandwidth B , except for those groups with $m = 0, m' = 0$, or $m = m'$. The DWTs are clustered according to the Wigner- d symmetries (3). ① The triangular area is divided into two parts by a cut at halfway along the m axis. ② The lower part of the triangular area is mirrored at both axes. ③ The mirrored area fits in the empty space in the upper half of the square with side length $B - 1$ containing the original triangle. The resulting rectangle can be worked through using two independent indices i and j . In doing so, the groups with $m = m'$ are skipped. We treat these cases separately because not all seven Wigner- d symmetries (3) are meaningful for these groups. The same applies to the groups with $m = 0$ or $m' = 0$, which we also treat in advance.

The following test was performed for the bandwidths 32, 64, 128, 256, and 512, each with the sequential algorithms as well as the parallel algorithms with two through 64 computation nodes (cores): 1) Generate random complex Fourier coefficients $f^\circ(l, m, m')$, the real and imaginary part being both uniformly distributed on $[-1, 1]$. 2) Reconstruct the corresponding function values $f(\alpha_i, \beta_j, \gamma_k)$ using the fast sequential as well as the parallel iFSOFT. 3) Compute reconstructed Fourier coefficients $f^*(l, m, m')$ using the fast sequential as well as the parallel FSOFT.

The speedup of the parallel FSOFT and iFSOFT is shown in Fig. 2. The underlying runtime is depicted in Fig. 3. The efficiency of our parallelization is presented in Fig. 4. Table 1 shows the maximum absolute and relative transformation error,

$$\max_{|m|, |m'| \leq l < B} |(f^\circ - f^*)(l, m, m')| \quad \text{and} \quad \max_{|m|, |m'| \leq l < B} \frac{|(f^\circ - f^*)(l, m, m')|}{|f^\circ(l, m, m')|},$$

respectively, measured in the above benchmark test.

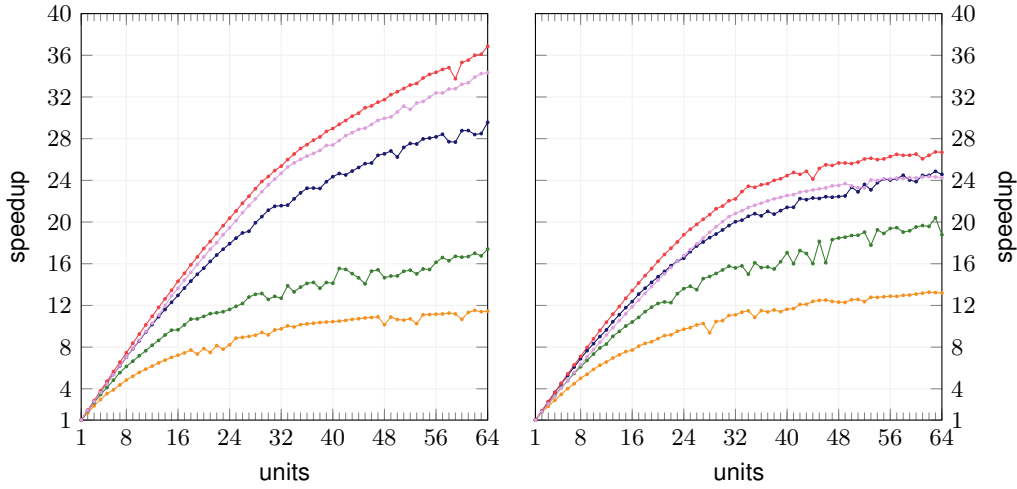


Fig. 2. Speedup of the (left) parallel FSOFT and (right) parallel iFSOFT. Orange (■) is for the bandwidth 32, green (■) for the bandwidth 64, blue (■) for the bandwidth 128, red (■) for the bandwidth 256, and purple (■) for the bandwidth 512.

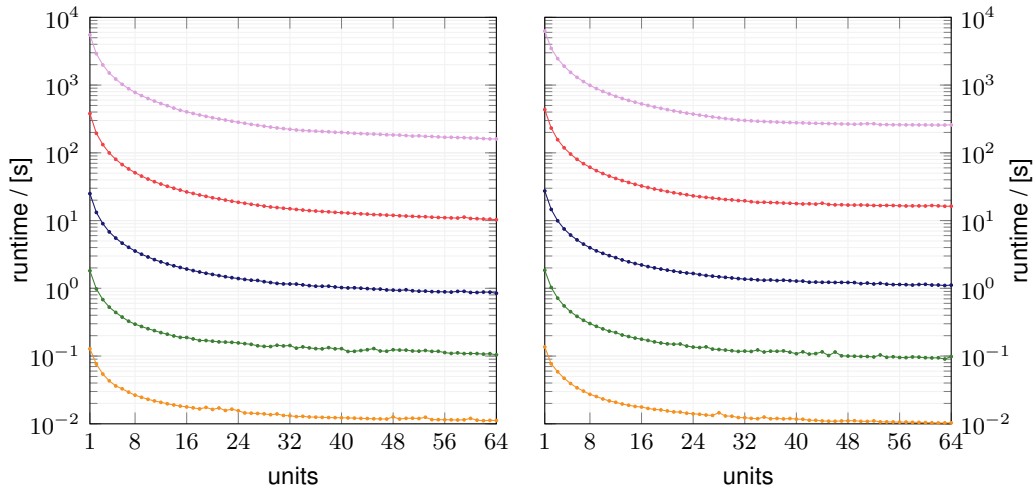


Fig. 3. Runtime (logarithmically plotted) of the (left) parallel FSOFT and (right) parallel iFSOFT. Orange (■) is for the bandwidth 32, green (■) for the bandwidth 64, blue (■) for the bandwidth 128, red (■) for the bandwidth 256, and purple (■) for the bandwidth 512.

5. DISCUSSION

The results of the benchmark test clearly show that our parallelization of the FSOFT and iFSOFT was successful, and that current and future applications can benefit considerably from these novel parallel algorithms and our corresponding C++ implementation using OpenMP.

As can be seen by having a closer look at the speedup depicted in Fig. 2, the beneficial impact of our parallelization initially increases fast with the bandwidth, especially when many nodes are used. This effect is stronger in the forward than in the inverse

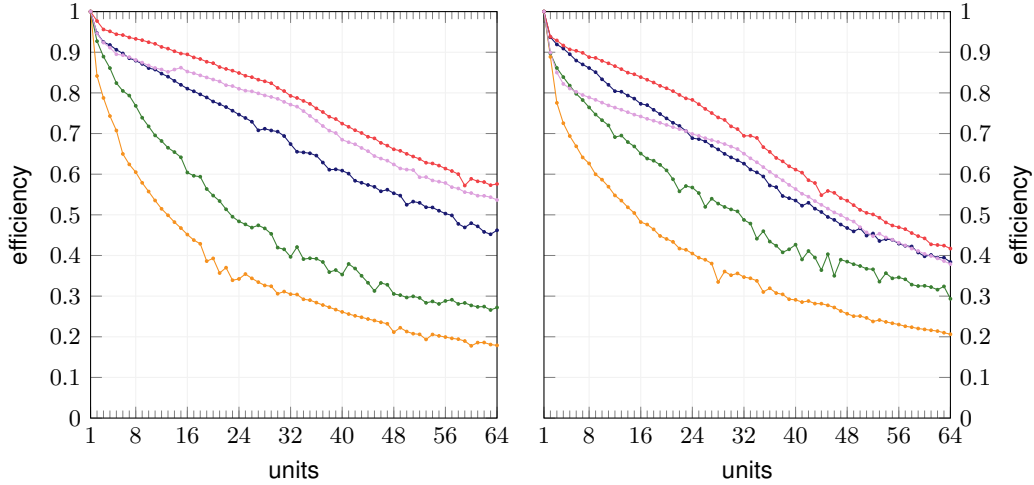


Fig. 4. Efficiency of the **(left)** parallel FSOFT and **(right)** parallel iFSOFT. Orange (■) is for the bandwidth 32, green (■) for the bandwidth 64, blue (■) for the bandwidth 128, red (■) for the bandwidth 256, and purple (■) for the bandwidth 512.

B	maximum absolute error	maximum relative error
32	$(1.10 \pm 0.14)E - 14$	$(7.91 \pm 7.85)E - 13$
64	$(2.79 \pm 0.23)E - 14$	$(3.08 \pm 2.31)E - 12$
128	$(6.23 \pm 0.65)E - 14$	$(1.89 \pm 1.33)E - 11$
256	$(2.21 \pm 0.13)E - 13$	$(9.21 \pm 4.57)E - 11$
512	$(4.98 \pm 0.33)E - 13$	$(4.26 \pm 2.73)E - 10$

Table 1. Maximum absolute and relative error of an iFSOFT and subsequent FSOFT, averaged over ten runs for each bandwidth.

transform. The results suggest that there is a limiting bandwidth to this effect, however—in both the forward and inverse transform, the bandwidth 512 already presents a slightly lower speedup than the bandwidth 256; this can be attributed to increased side effects (see below). The runtime of the iFSOFT was generally longer than that of the FSOFT (see Fig. 3). The reason for this is the matrix transposition in the current version of the iDWT. This transposition of matrices of strongly varying size is performed on-the-fly by the computation nodes, which especially in the larger bandwidths results in a lower speedup in the inverse transform due to common side effects such as increasing workload imbalance and memory management overhead. The time for computing the $SO(3)$ quadrature weights (6) in the forward transform, on the other hand, is negligible short. Generally, in all bandwidths considered, the speedup initially increases fast with the number of computation nodes, and in the larger bandwidths 128, 256, and 512 even almost reaches its optimum (equal to the number of computation nodes), until around eight nodes. Subsequently, the speedup begins to plateau, again due to influencing factors such as increasingly complicated memory management, etc. This is also reflected in the naturally decreasing efficiency shown in Fig. 4. While it is conceivable that our parallel algorithms will benefit from employing more nodes than available on our testing system, the results overall suggest that it would be of no avail

to recruit a very much higher number of computation nodes with a comparable system architecture, at least until a faster DWT/iDWT is used.

As indicated above, an elaborate parallelization of the two-dimensional FFT/iFFT is beyond the scope of this paper. Works on parallelization of the classical FFTs include [Bahn et al. 2008; Agarwal et al. 1994; Averbuch et al. 1990]. Although the speedup achieved in these works cannot directly be compared with that in our case, it is interesting to see the very similar behavior in [Bahn et al. 2008, Fig. 5] (note that the number of relevant SO(3) Fourier coefficients for the bandwidth B is $B(4B^2 - 1)/3$, while the number of Fourier coefficients in a classical three-dimensional FFT with bandwidth N is N^3 . Moreover, the cost is different for computing a single Fourier coefficient because the more demanding DWT replaces a classical DFT, simply put). It is noteworthy that particularly in the larger bandwidths, the runtime of the parallel two-dimensional iFFT/FFT proposed by the FFTW developers constituted only small portion of the total runtime of the FSOFT/iFSOFT in our benchmark test (approximately 5% and 8%, respectively, for the bandwidth 512 when using all 64 cores).

Apart from our parallelization, an additional contribution of this paper to computational harmonic analysis on SO(3) in general is our treatment of the both accuracy- and memory-critical bandwidth 512. To our knowledge, this large bandwidth has not been attempted by others before (compare especially [McEwen et al. 2015; Potts et al. 2009; Kostelec and Rockmore 2008]). The results of the error measurement in Table 1 show that we were successful in performing the full forward and inverse transform for this large bandwidth. This is due to the large amount of RAM available on our testing system and, more importantly, the fact that we increased from double to extended double precision (double precision is not sufficient). The errors shown in Table 1 for the other bandwidths are much smaller than those in [Kostelec and Rockmore 2008, Table 7]; they are not directly comparable with those in [Potts et al. 2009, Fig. 6], because the error was defined differently by these authors. As mentioned above, the bandwidth 512 also benefits greatly from our parallelization, resulting in a speedup of 34.34 (forward) and 24.25 (inverse) using all 64 available cores, resulting from a runtime of approximately three minutes (forward) and 4.3 minutes (inverse) as opposed to 1.53 hours (sequential forward) and 1.74 hours (sequential inverse).

Now that we realized our idea and demonstrated its feasibility as a general proof of concept already showing practical applicability, the next version of our software will include a faster DWT/iDWT based on Clenshaw's algorithm [1955].

REFERENCES

- Milton Abramowitz and Irene A. Stegun (eds.). 1972. *Handbook of Mathematical Functions with Formulas, Graphs, and Mathematical Tables* (10. ed.). US Department of Commerce, National Bureau of Standards, Gaithersburg, MD, USA.
- Ramesh C. Agarwal, Fred G. Gustavson, and Mohammad Zubair. 1994. A high performance parallel algorithm for 1-d FFT. In *Proceedings of Supercomputing*. Washington, DC, USA, 34–40.
- Amir Averbuch, Eran Gabber, Boaz Gordissky, and Yoav Medan. 1990. A parallel FFT on an MIMD machine. *Parallel Comput.* 15(1):61–74.
- Lionel Baboud, Martin Čadík, Elmar Eisemann, and Hans-Peter Seidel. 2011. Automatic photo-to-terrain alignment for the annotation of mountain pictures. In *Proceedings of the IEEE Conference on Computer Vision and Pattern Recognition (CVPR)*. Providence, RI, USA, 41–48.
- Jun H. Bahn, Jung S. Yang, and Nader Bagherzadeh. 2008. Parallel FFT algorithms on network-on-chips. In *Fifth International Conference on Information Technology: New Generations (ITNG)*. Las Vegas, NV, USA, 1087–1093.
- Chandrajit L. Bajaj, Benedikt Bauer, Radhakrishna Bettadapura, and Antje Vollrath. 2013. Nonuniform Fourier transforms for rigid-body and multidimensional rotational correlations. *SIAM J. Sci. Comput.* 35(4):B821–B845.
- Chandrajit L. Bajaj, Rezaul Chowdhury, and Vinay Siddahanavalli. 2011. F²Dock: fast Fourier protein-protein docking. *IEEE/ACM Trans. Comput. Biol. Bioinform.* 8(1):45–58.

- Tejal Bhamre, Teng Zhang, and Amit Singer. 2015. Orthogonal matrix retrieval in cryo-electron microscopy. In *Proceedings of the 12th IEEE International Symposium on Biomedical Imaging (ISBI)*. Brooklyn Bridge, NY, USA, 1048–1052.
- Heiko Bülow and Andreas Birk. 2011a. Spectral registration of noisy sonar data for underwater 3D mapping. *Auton. Robots* 30(3):307–331.
- Heiko Bülow and Andreas Birk. 2011b. Spectral registration of volume data for 6-DOF spatial transformations plus scale. In *Proceedings of the IEEE International Conference on Robotics and Automation (ICRA)*. Shanghai, China, 3078–3083.
- Charles W. Clenshaw. 1955. A note on the summation of Chebyshev series. *Math. Comp.* 9(51):118–120.
- Anthony Crowther. 1972. The fast rotation function. In *The Molecular Replacement Method*, M G Rossmann (ed.). Gordon & Breach, 173–178.
- James R. Driscoll, Dennis M. Healy, and Daniel N. Rockmore. 1997. Fast discrete polynomial transforms with applications to data analysis for distance transitive graphs. *SIAM J. Comput.* 26(4):1066–1099.
- Alan R. Edmonds. 1996. *Angular Momentum in Quantum Mechanics*. Princeton University Press, Princeton, NJ, USA.
- Felcy Fabiola and Michael S. Chapman. 2005. Fitting of high-resolution structures into electron microscopy reconstruction images. *Structure* 13(3):389–400.
- Ian Forster. 1995. *Designing and Building Parallel Programs: Concepts and Tools for Parallel Software Engineering*. Addison-Wesley, Boston, MA, USA.
- José I. Garzon, José R. Lopéz-Blanco, Carles Pons, Julio Kovacs, Ruben Abagyan, Juan Fernandez-Recio, and Pablo Chacon. 2009. FRODOCK: a new approach for fast rotational protein-protein docking. *Bioinformatics* 25(19):2544–2551.
- Joseph JáJá. 1992. *An Introduction to Parallel Algorithms*. Addison Wesley Longman Publishing Co., Inc., Redwood City, CA, USA.
- Zvi Kam. 1980. The reconstruction of structure from electron micrographs of randomly oriented particles. *J. Theor. Biol.* 82(1):15–39.
- Michael Kazhdan. 2007. An approximate and efficient method for optimal rotation alignment of 3d models. *IEEE Trans. Pattern Anal. Mach. Intell.* 29(7):1221–1229.
- Michael Kazhdan, Thomas Funkhouser, and Szymon Rusinkiewicz. 2003. Rotation invariant spherical harmonic representation of 3d shape descriptors. In *Proceedings of the 2003 Eurographics/ACM SIGGRAPH symposium on geometry processing (SGP)*. Aire-la-Ville, Switzerland, 156–164.
- Peter J. Kostelec and Daniel N. Rockmore. 2008. FFTs on the rotation group. *J. Fourier Anal. Appl.* 14(2):145–179.
- Julio A. Kovacs and Willy Wriggers. 2002. Fast rotational matching. *Acta Cryst.* D58(8):1282–1286.
- Alexander B. Kyatkin and Gregory S. Chirikjian. 2000. Algorithms for fast convolutions on motion groups. *Appl. Comput. Harmon. Anal.* 9(2):220–241.
- Denis-Michael Lux. 2015. A parallelization of the fast Fourier transform on SO(3). Bachelor’s thesis (in German). Institute of Mathematics, Lübeck University. http://www.math.uni-luebeck.de/mitarbeiter/wuelker/Bachelor_thesis_Lux.pdf.
- Gary Macindoe, Lazaros Mavridis, Vishwesh Venkatraman, Marie-Dominique Devignes, and David W. Ritchie. 2010. HexServer: an FFT-based protein docking server powered by graphics processors. *Nucleic Acids Research* 38(Suppl. 2):W445–W449.
- Ameesh Makadia and Kostas Daniilidis. 2006. Rotation recovery from spherical images without correspondences. *IEEE Trans. Pattern Anal. Mach. Intell.* 28(7):1170–1175.
- Ameesh Makadia and Kostas Daniilidis. 2010. Spherical correlation of visual representations for 3d model retrieval. *Int. J. Comput. Vis.* 89(2):193–210.
- Ameesh Makadia, Lorenzo Sorgi, and Kostas Daniilidis. 2004. Rotation estimation from spherical images. In *Proceedings of the 17th International Conference on Pattern Recognition (ICPR)*, Vol. 3. Cambridge, UK, 590–593.
- Ameesh Makadia, Mirko Visontai, and Kostas Daniilidis. 2007. Harmonic silhouette matching for 3d models. In *Proceedings of the 3DTV conference*. Kos Island, Greece, 1–4.
- Lazaros Mavridis, Brian D. Hudson, and David W. Ritchie. 2007. Toward high throughput 3d virtual screening using spherical harmonic surface representations. *J. Chem. Inf. Model.* 47(5):1787–1796.
- Jason D. McEwen, Martin Büttner, Boris Leistedt, Hiranya V. Peiris, and Yves Wiaux. 2015. A novel sampling theorem on the rotation group. *IEEE Signal Process. Lett.* 22(12):2425–2429.
- Jorge Navaza. 1993. On the computation of the fast rotation function. *Acta Cryst.* D49(6):588–591.
- Daniel Potts, Jürgen Prestin, and Antje Vollrath. 2009. A fast algorithm for nonequispaced Fourier transforms on the rotation group. *Numer. Algorithms* 52(3):355–384.
- Daniel Potts, Gabriele Steidl, and Manfred Tasche. 1998. Fast algorithms for discrete polynomial transforms. *Math. Comp.* 67(224):1577–1590.
- Michael J. Quinn. 2003. *Parallel Programming in C with MPI and OpenMP*. The McGraw-Hill Companies, Inc., New York, NY, USA.

- David W. Ritchie, Dima Kozakov, and Sandor Vajda. 2008. Accelerating and focusing protein-protein docking correlations using multi-dimensional rotational FFT generating functions. *Bioinformatics* 24(17):1865–1873.
- David W. Ritchie and Vishwesh Venkatraman. 2010. Ultra-fast FFT protein docking on graphics processors. *Bioinformatics* 26(19):2398–2405.
- Seyed H. Roosta. 2000. *Parallel Processing and Parallel Algorithms*. Springer-Verlag New York, Inc., New York, NY, USA.
- Greg Slabaugh, Tong Fang, Fred McBagonluri, Alexander Zouhar, Rupen Melkisetoglu, Hui Xie, and Gozde Unal. 2008. 3-d shape modeling for hearing aid design. *IEEE Signal Process. Mag.* 25(5):98–102.
- Laurent C. Storoni, Airlie J. McCoy, and Randy J. Read. 2004. Likelihood-enhanced fast rotation functions. *Acta Cryst.* D60(3):432–438.